



## Evidence for fluid and melt generation in response to an asthenospheric upwelling beneath the Hangai Dome, Mongolia

Matthew J. Comeau <sup>a,\*</sup>, Johannes S. Käufl <sup>b</sup>, Michael Becken <sup>a</sup>, Alexey Kuvshinov <sup>b</sup>, Alexander V. Grayver <sup>b</sup>, Jochen Kamm <sup>a</sup>, Sodnomsambuu Demberel <sup>c</sup>, Usnikh Sukhbaatar <sup>c</sup>, Erdenechimeg Batmagnai <sup>c</sup>

<sup>a</sup> Institut für Geophysik, Universität Münster, Correnstrasse 24, Münster, 48149, Germany

<sup>b</sup> Institute of Geophysics, Swiss Federal Institute of Technology (ETH), Sonneggstrasse 5, Zürich, 8092, Switzerland

<sup>c</sup> Institute of Astronomy & Geophysics, Mongolian Academy of Sciences, P.O.B-152, Ulaanbaatar, 13343, Mongolia



### ARTICLE INFO

#### Article history:

Received 24 November 2017

Received in revised form 1 February 2018

Accepted 5 February 2018

Available online xxxx

Editor: P. Shearer

#### Keywords:

magnetotellurics

electrical resistivity

Mongolia

Hangai

partial melt

intratplate volcanism

### ABSTRACT

The Hangai Dome, Mongolia, is an unusual high-elevation, intra-continental plateau characterized by dispersed, low-volume, intraplate volcanism. Its subsurface structure and its origin remains unexplained, due in part to a lack of high-resolution geophysical data. Magnetotelluric data along a ~610 km profile crossing the Hangai Dome were used to generate electrical resistivity models of the crust and upper mantle. The crust is found to be unexpectedly heterogeneous. The upper crust is highly resistive but contains several features interpreted as ancient fluid pathways and fault zones, including the South Hangai fault system and ophiolite belt that is revealed to be a major crustal boundary. South of the Hangai Dome a clear transition in crustal properties is observed which reflects the rheological differences across accreted terranes. The lower crust contains discrete zones of low-resistivity material that indicate the presence of fluids and a weakened lower crust. The upper mantle contains a large low-resistivity zone that is consistent with the presence of partial melt within an asthenospheric upwelling, believed to be driving intraplate volcanism and supporting uplift.

© 2018 Elsevier B.V. All rights reserved.

## 1. Introduction

The Hangai Dome in central Mongolia is an uplifted, intra-continental plateau with a large topographic bulge extending more than 2000 m above the regional elevation (Cunningham, 2001). The mechanism of uplift and support in the continental interior, away from active tectonic margins, is an open and important question. The Hangai region occupies a unique position in central Asia because it is a link between actively deforming regions. It is located between the rigid Siberian craton to the north, which is associated with an east-west extensional regime near the Baikal rift, and the North China and Tarim cratons to the south (see Fig. 1), which have a northward compressional regime to accommodate the movement of the Tibetan Plateau from the India–Asia collision (e.g., Calais et al., 2003). The Hangai region is believed to be underlain by a rigid pre-Cambrian crustal block (Cunningham, 2001). It is bounded by large, seismically active faults (Walker et al., 2007) that, along with the transpressional deformation of the Altai range, accom-

modate the northward compressional motion (Cunningham, 2001; Calais et al., 2003). Both the Bulnay fault system to the north and the Bogd fault system to the south have had intra-continental earthquakes larger than magnitude 8 within the last century (e.g., Calais et al., 2003, and references therein).

Magmatism is commonly associated with tectonic plate boundary processes, such as subduction and rifting. Enigmatically, intra-continental, intraplate volcanism occurs throughout the Hangai region. It is characterized by dispersed, low-volume, alkali basaltic volcanism, with ages from the Holocene to the Oligocene (2 ka to 33 Ma) (Barry et al., 2003). The onset of uplift and doming is believed to have been coincident with the beginning of volcanism (e.g., Cunningham, 2001; Walker et al., 2007; Sahagian et al., 2016), indicating that the processes may be linked. A mantle plume was originally favored to explain the origin of the high topography and associated volcanism far from active tectonic margins (Windley and Allen, 1993). However, some recent petrological evidence is inconsistent with a deep-rooted, high heat-flux mantle plume, including: dispersed volcanism that exhibits no definable spatial boundaries and lacks age progression, small erupted volumes that occurred sporadically, and a lack of xenolith evidence

\* Corresponding author.

E-mail address: matthew.comeau@uni-muenster.de (M.J. Comeau).

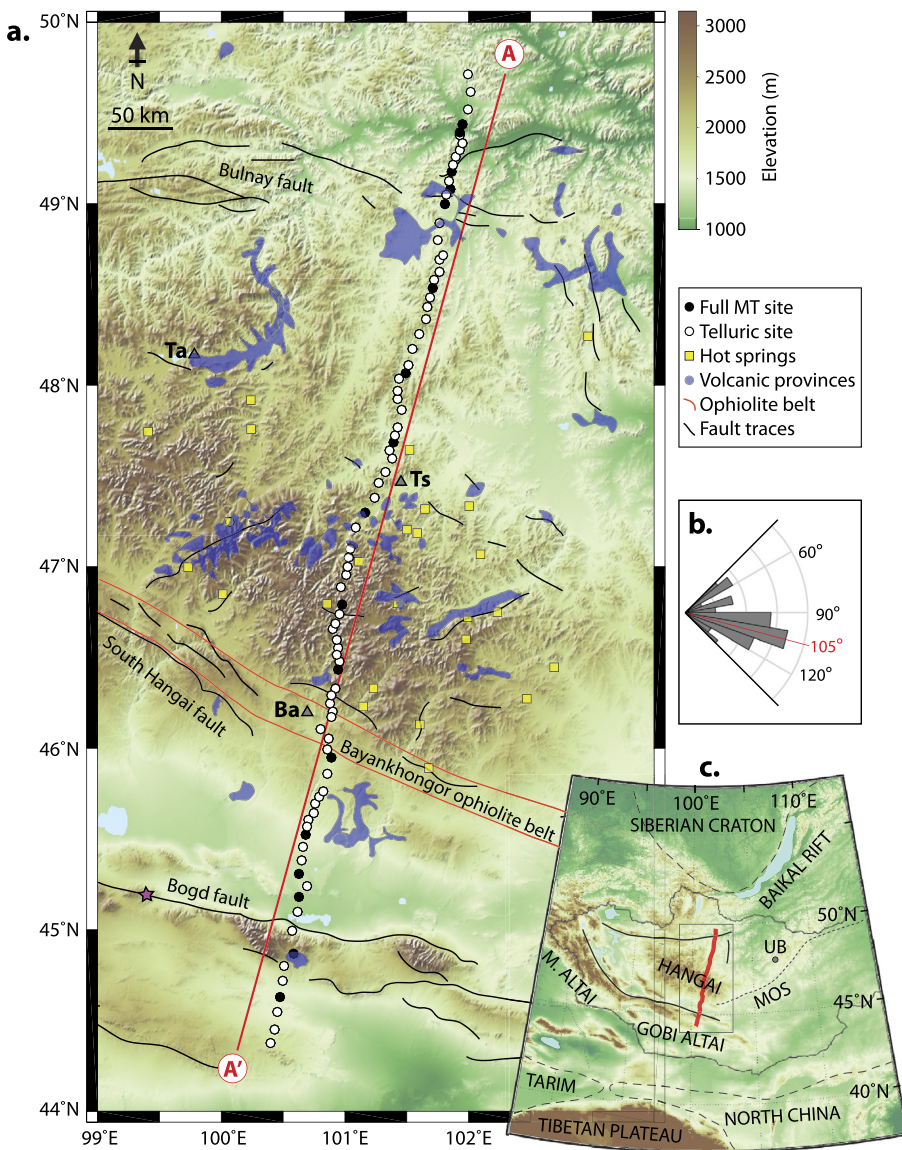


**Fig. 1.** (a) Topographic map of the study area. A total of 89 magnetotelluric (MT) sites (circles) were deployed along profile A–A' (red line). Select towns are shown for reference: Ba = Bayankhongor, Ta = Tariat, Ts = Tssetsrleg. Additional information includes: volcanic provinces (blue shapes) (adapted from Sahagian et al., 2016; Hunt et al., 2012, and Cunningham, 2001); hot springs (gold squares) (Ganbat and Demberel, 2010); fault traces (black lines) (adapted from Walker et al., 2007, 2008); ophiolite belt (orange lines) (Badarch et al., 2002); pink star marks the epicenter of the 1957 Bogd event (Calais et al., 2003). (b) Average 2-D geo-electric strike direction calculated from the MT data, for periods of 1–1000 s. (c) The Hangai region has a unique position between the Siberian craton and the North China and Tarim cratons (dashed gray lines) (Badarch et al., 2002). The survey location (box), MT sites (red dots), Mongolian Altai and Gobi Altai mountains, political boundary of Mongolia (thin black line), and the capital city, Ulaanbataar (UB), are indicated. Major fault systems (solid black lines) bound the Hangai region (Walker et al., 2007). The approximate location of the Mongol-Okhotsk suture zone (MOS; dotted gray line) is marked (Van der Voo et al., 2015).

for anomalously high lithospheric temperatures (Barry et al., 2003; Harris et al., 2010). Hence alternative explanations are sought.

Seismic studies, supported by analysis of xenoliths from surface lavas, estimated a surprisingly thin lithosphere (60–80 km) below the central Hangai region, in comparison to the surrounding area (120–225 km) (Petit et al., 2008; Ionov, 2002). In addition, they detected a thick crust (45–55 km) below the Hangai region which thins at the edges (~35 km) (Petit et al., 2008). Other geophysical studies have determined that the lithosphere below the Hangai Dome has anomalously low seismic velocities (e.g., Chen et al., 2015), and is characterized by a very low negative Bouguer anomaly (<−250 mGal) compared to the surrounding region (Tiberi et al., 2008). However the lithospheric structure of the Hangai region is poorly understood and additional high-resolution geophysical data are needed to give detailed images of subsurface

structures, specifically crustal features, and to gain further insights into its origin.

Magnetotelluric (MT) data map subsurface electrical resistivity using natural electromagnetic signals (e.g., Chave and Jones, 2012). The resistivity of a rock is highly sensitive to the quantity and composition of fluids, and hence the MT method is useful for investigating subsurface fluid and melt distribution. Therefore MT data have the potential to image intraplate volcanism throughout the lithospheric column and to restrict the mechanisms responsible for the uplift and support of the Hangai Dome. Moreover, MT data can help to provide constraints on lithospheric viscosity and mechanical strength, both of which are required for accurate modeling of lithosphere dynamics (Liu and Hasterok, 2016). Although the Hangai region is unique, its origin is relevant for other cases of continental uplift and intraplate volcanism worldwide, over diverse scales and settings, such as south-eastern Australia (e.g.,

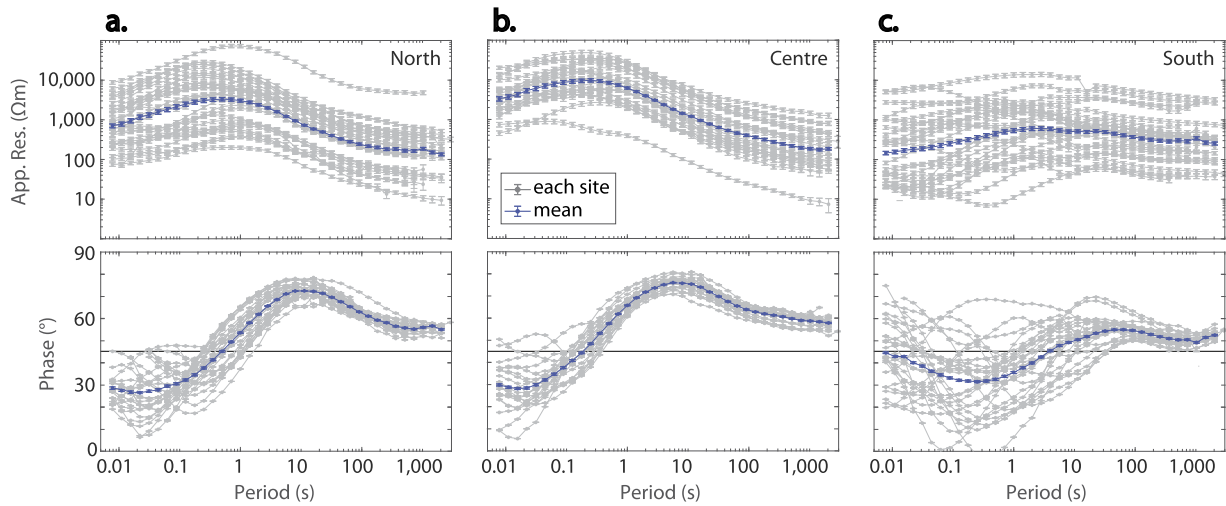


**Fig. 2.** Apparent resistivity and phase curves from the ssq-average for all individual magnetotelluric sites (gray lines) and their geometric mean (blue lines) from three regions: north of the Hangai Dome (a), across it (b), and south of it (c). (For interpretation of the references to color in this figure, the reader is referred to the web version of this article.)

Aivazpourporgou et al., 2015) and the Colorado Plateau, USA (e.g., Wannamaker et al., 2008).

## 2. Magnetotelluric data

### 2.1. Data collection and analysis

In 2016 and 2017 MT data were collected across west-central Mongolia in order to investigate the electrical resistivity beneath the Hangai region, the first survey of its kind in Mongolia. A  $\sim 610$  km profile crossing the Hangai Dome (A-A', 89 sites; Fig. 1a) will be the focus of this paper, with future work concentrating on several parallel profiles to the west and a three-dimensional (3-D) analysis of the entire dataset. Telluric-only dataloggers, developed by the University of Münster, were deployed with 5–10 km spacing, and were accompanied by broadband and long-period full MT instruments, provided by the Geophysical Instrument Pool Potsdam (GIPP), with a nominal spacing of 50 km. Inter-site transfer functions were computed between the telluric-only sites and the full MT sites (e.g., Munoz and Ritter, 2013). This setup allowed fast and efficient data collection in the field. MT site occupation times were on average 4 days for broadband and telluric-only sites and 20 days for long-period sites. The total period range recorded was 0.002–12,000 s, with long period data up to 3000 s obtained at most MT sites (see Fig. 2), providing penetration to upper mantle depths. The MT data were high quality and had a very low noise level due to the remote measurement location.

In order to better understand the MT data, the survey area was separated into three segments: across the Hangai Dome, north of it, and south of it. For each MT site the sum of the squared elements of the impedance tensor (ssq-average) and their geometric mean were calculated (Rung-Arunwan et al., 2016). The geometric mean represents a regional one-dimensional (1-D) average and is assumed to average out any static shift, which is a constant, frequency-independent offset of the apparent resistivity caused by near-surface resistivity structure that occurs at a small spatial length scale (e.g., Chave and Jones, 2012). This analysis illustrated the consistency of the apparent resistivity and phase curves in the northern and central regions despite large (two orders of magnitude) static shift effects, but revealed some prominent differences in the southern region (see Fig. 2).

A dimensionality analysis of the MT data was performed using tensor decomposition and phase tensor methods (e.g., McNeice

and Jones, 2001; Chave and Jones, 2012). The data show an average regional geo-electric strike direction of N100°E–N110°E, over periods of 1–1000 s (Fig. 1b; Fig. S1). The strike direction is plausible because it is approximately orogen-parallel ( $\sim$ N110°E), comparable to the main fault systems in the area (N100°E–N120°E) (e.g., Walker et al., 2007), and consistent with seismic anisotropy results (N115°E–N135°E) (Barruol et al., 2008). The dimensionality analysis established that a two-dimensional (2-D) model is largely valid, although certain regions displayed distortion or local 3-D resistivity structures (Figs. S2b and S3), specifically the central region of the profile, below the Hangai Dome, and the southern portion of the profile near the Gobi Altai mountains.

### 2.2. Data modeling

Regional 1-D electrical resistivity models were produced by inverting the geometric mean of the sum of the squared elements of the impedance tensor (ssq) (Rung-Arunwan et al., 2016) computed from the MT data (see Fig. 2). The 1-D inversion is based on a probabilistic algorithm that finds the best fitting model in a first step and then samples a number of probable (i.e., low misfit) models in a second step, in order to quantify the uncertainty of the solution (Grayver and Kuvshinov, 2016). The 1-D models allow the dominant features of the MT data to be identified (Fig. 3a). By separating the survey area into three segments across the Hangai region the models illustrate the differences between the segments and the uncertainty within each segment.

Next, a 2-D electrical resistivity model was created from the MT data (Fig. 3d) by applying the EMILIA inversion algorithm from Kalscheuer et al. (2010), which is based on a damped Occam approach. Both modes of the impedance tensor were inverted: the transverse electric mode (TE; electric currents flowing along strike, perpendicular to the profile) and the transverse magnetic mode (TM; electric currents flowing across strike). Importantly, the algorithm was capable of properly handling inter-site transfer functions computed for the telluric-only sites. The data were rotated to a strike direction of N105°E (that is, the TE component was aligned in this direction). The starting model included two layers designed to simulate the approximate lithosphere–asthenosphere boundary: a resistive layer of 1000  $\Omega\text{m}$  to 100 km depth overlying a homogeneous half-space of 100  $\Omega\text{m}$ . Model columns were 1100 m wide across the survey area and model rows increased geometrically from a thickness of 100 m. All model depths are below the average surface elevation, defined as 2000 m. Periods in the range

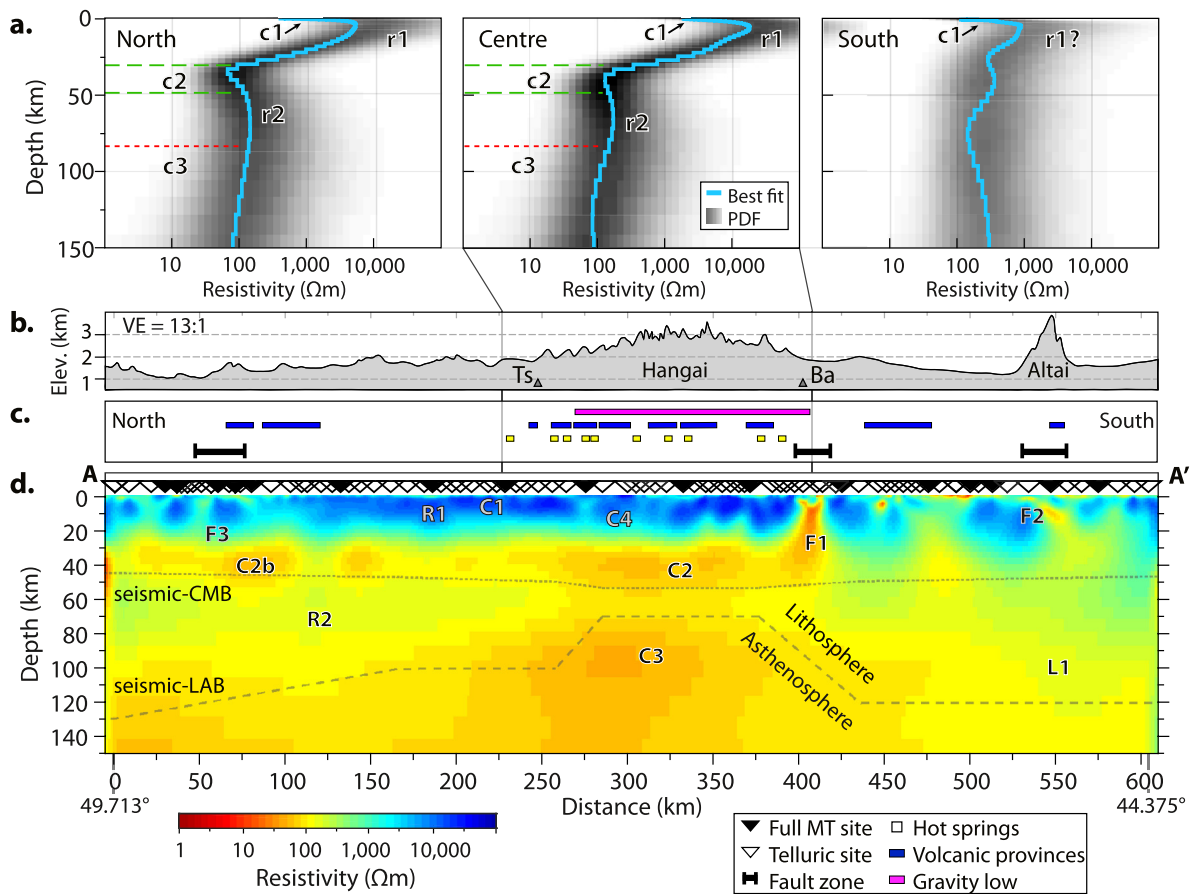


**Fig. 3.** (a) The 1-D inversion models obtained from the averaged responses for each segment of the Hangai region. Blue line indicates the best fit model and the gray cloud represents the probability density function (PDF) for multiple low-misfit models. In the region between the dashed green lines ( $\sim 30$ – $50$  km depth; c2) and below the dotted red line ( $\sim 80$  km; c3) the resistivity drops below  $\sim 150 \Omega\text{m}$ . (b) Elevation along profile A–A'. Note there is a vertical exaggeration of 13:1. Select towns are shown for reference: Ba = Bayankhongor, Ts = Tsetserleg. (c) Additional information projected onto the profile: low Bouguer gravity anomaly (pink) (Tiberi et al., 2008); volcanic provinces (blue) (Sahagian et al., 2016; Hunt et al., 2012); hot Bouguer gravity anomalies (gold) (Ganbat and Demberel, 2010); main fault zones (black) (Walker et al., 2007, 2008). (d) The resistivity model obtained from the 2-D inversion of magnetotelluric (MT) data at 89 sites (triangles) along profile A–A' (see Fig. 1 for location). Distances along the profile, from north to south, and latitudes are marked. The approximate location of the seismically-inferred crust–mantle boundary (seismic-CMB; dotted line) and the simplified seismically-inferred lithosphere–asthenosphere boundary (seismic-LAB; dashed line) are indicated (Petit et al., 2008).

of 0.0078 to 10,000 s were inverted. Both TE and TM mode phase components were assigned an error floor of 1.4°, and the TM mode apparent resistivity was assigned an error floor of 10%. The TE mode apparent resistivity was assigned a high error floor of 100% in order to reduce the influence of the static shift effect (e.g., Chave and Jones, 2012), by allowing the TE mode apparent resistivity to be shifted for all frequencies by a constant factor (see Fig. S4). The inversion algorithm smoothly converged after 12 iterations with the total root-mean-square (RMS) misfit reduced from 12.42 to 2.75, indicating that the model fits the measured MT data (Fig. 4). Note that the total misfit was significantly influenced by the high frequency data because the variable very near-surface layer was difficult to fit uniformly between sites. This was demonstrated by inverting the longer period data only (10–10,000 s), which gave a total RMS misfit of 1.74. The fit is fairly evenly spread across all sites, indicating that the model is not biased to some section of the data (Fig. S5).

Many combinations of inversion model parameters were thoroughly investigated, and it was found that the main resistivity features of the model did not depend on any specific choice of parameters. For example, no significant changes in the main model features were observed when the geo-electric strike angle was varied by  $\pm 15^\circ$ , or the starting model was set to a simple half-space, although the model RMS misfit increased by up to 15%. Model resolution and sensitivity were investigated systematically using synthetic inversions. The robustness of model features were tested

in several ways, including by removing them from the model and comparing the data fit, and by re-inverting to test if the features were re-introduced (Fig. S6). These tests proved that the model's main features are all required. Crustal features of the model are particularly well-constrained.

### 3. Results and discussion

#### 3.1. Modeling results

Features of the 1-D and 2-D resistivity models derived from the MT data (Fig. 3) are described here and discussed in more detail below. Low-resistivity (conductive) anomalies can have many causes, including aqueous fluids, partial melts, or hydrothermal alteration, and therefore any interpretation must use additional information to distinguish between the possibilities (e.g., Chave and Jones, 2012; Unsworth and Rondenay, 2012). The near-surface layer (C1;  $< 0.5$  km) has a highly variable resistivity (10–2000  $\Omega\text{m}$ ) and is likely caused by porous sediments (Ganbat and Demberel, 2010). It is underlain by an upper crustal resistor (R1; 2000–40,000  $\Omega\text{m}$ ) that can be explained by highly-resistive, pre-Cambrian, cratonic basement rocks (Cunningham, 2001). A heterogeneous zone that contains pockets of relatively low-resistivity material (C2; 20–80  $\Omega\text{m}$ ) is imaged below the Hangai Dome at lower crustal depths of 30–50 km. Although this is not considered highly conductive, and increased conductivity in the lower crust

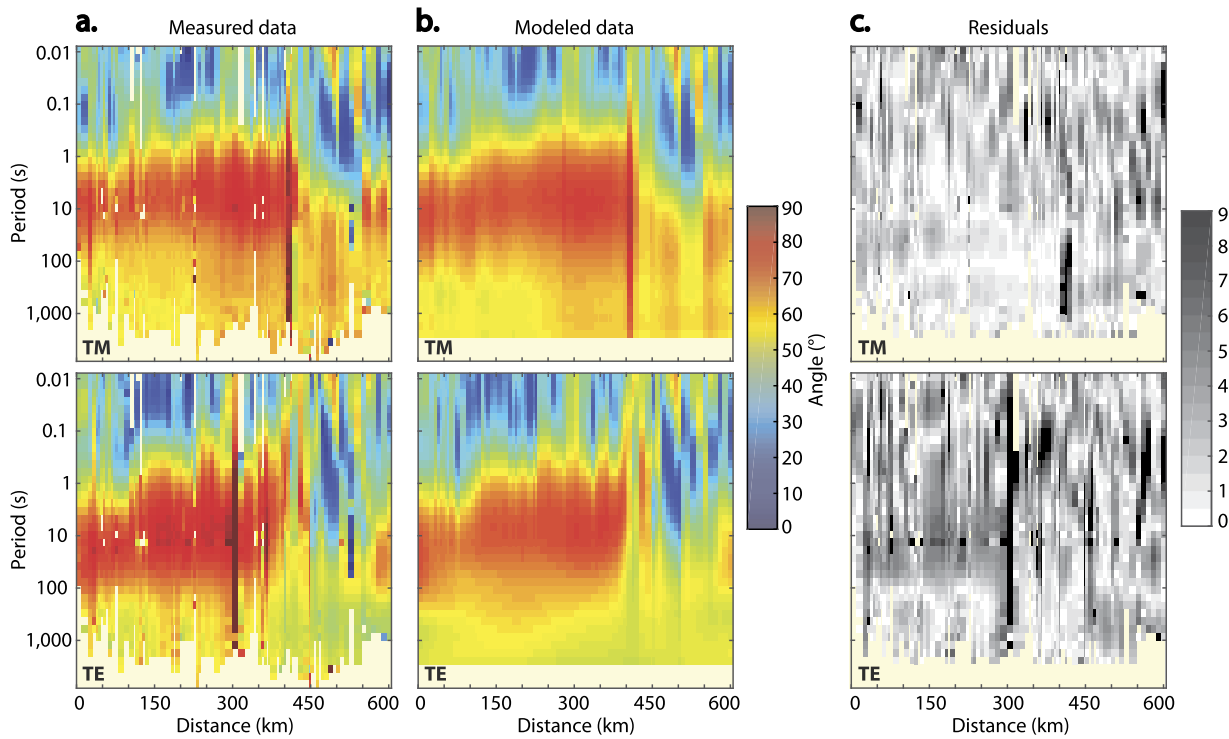


**Fig. 4.** Pseudosections of the impedance phase from the measured magnetotelluric data (a) and the modeled data (b), for TM mode (top row) and TE mode (bottom row). Residuals (c), the difference of the modeled data from the measured data, are error-normalized and illustrate that the model fits the data.

has been detected elsewhere (e.g., Ritter et al., 2003; Wannamaker et al., 2008), it is significant given its location within the highly resistive crustal craton ( $\sim 10,000 \Omega\text{m}$ ), and therefore acts as a relative conductor. Note this zone is absent south of the Hangai Dome, as clearly illustrated by the corresponding 1-D model.

Sub-crustal depths are characterized by a moderate resistivity (R2; 150–500  $\Omega\text{m}$ ) that represents the lithospheric mantle. At depths greater than  $\sim 70$  km (upper mantle) a large low-resistivity feature is imaged (C3; 30–60  $\Omega\text{m}$ ), embedded in a broad decrease in resistivity that represents the asthenosphere. MT data can give a reliable estimate of the depth to the top of a low-resistivity feature, but it is not always possible to detect its base because MT signals diffuse in the Earth and their depth of investigation is dependent on both the period of the electromagnetic fields measured and the resistivity of the medium. Therefore, the overall resolution is reduced below a depth of approximately 150 km (the skin depth for a resistivity of 30  $\Omega\text{m}$  and a period of 3000 s), and there is almost no resolution within or below the upper mantle feature C3.

### 3.2. Crustal structure

The lower crust beneath the Hangai Dome is a heterogeneous electrically conductive zone (C2). These features are well resolved by the dense MT site spacing. It is compatible with local, discrete accumulations of fluid or melt distributed and trapped within the lower crust. The conductive zone appears confined below the Hangai Dome (C2) and the northern part of the Hangai region (C2b); it is not observed south of the Hangai Dome. The depth to the top of this zone is coincident with the estimated brittle-ductile transition depth of 25 km (Deverchere et al., 2001), and crustal fluids tend to pool below this level (e.g., Connolly and Podlachikov, 2004). The results imply that a weak lower crust exists below the Hangai region. This must be considered in future geo-dynamic and mechanical models for the tectonics of the region, rather than assuming that the Hangai region acts as a homogeneous and rigid block. This result gives evidence for a significantly

reduced viscosity at depths of 30–50 km, as inferred from post-seismic deformation analysis and GPS data (Vergnolle et al., 2003). The positions of the heterogeneous discrete structures within this zone are robust because they are required in all modeling trials, including when a sparser MT site spacing is used, implying that they are likely not due to macro-anisotropy effects or inversion artefacts.

Geochemical evidence is inconsistent with long-lived crustal melt storage below the Hangai Dome. No significant spatial or temporal changes in the geochemistry of the lavas are observed across the Hangai Dome, and crustal assimilation and contamination appears limited, suggesting that all erupted magmas originated directly from a single parent source at mantle depths (Hunt et al., 2012). In addition, the presence of xenoliths indicate the ascent of magma from the mantle to the surface was very rapid (Harris et al., 2010). Magma traveled along pathways through the crust to surface vents, by dyking or along local crustal weaknesses such as re-activated faults (e.g., Cashman and Sparks, 2013). In fact, many volcanic provinces in the Hangai region are coincident with the location of known faults or inferred terrane boundaries (see Fig. 1). Although magma is likely no longer present in the crust, anomalous conductivity due to hydrothermal alteration from past eruptive events can be detected (e.g. Comeau et al., 2016; Hill et al., 2009). However, the rapid ascent of magma through the crust in transient pathways would not produce a very strong anomaly. Vertically elongated features observed in the upper crust (such as C4 in Fig. 3d; 400–1500  $\Omega\text{m}$ ) likely represent the electrical signatures of these past conduits of hot magma (see also Fig. S8). Their positions appear to be related to surface expressions of volcanism (Hunt et al., 2012; Sahagian et al., 2016) and present-day hydrothermal activity (Ganbat and Demberel, 2010).

Current heat flow measurements in this region are poor but indicate that the moderate values observed throughout Mongolia become elevated on the Hangai Dome, producing a higher crustal geothermal gradient (Ionov, 2002, and references therein), indicative of advective heat transfer. Present-day hydrothermal activ-

ity is observed across the Hangai Dome as meteoric hot springs (Oyuntsetseg et al., 2015; Ganbat and Demberel, 2010), and these regions are coincident with reduced very near-surface resistivity (<200  $\Omega\text{m}$ ; see Fig. S8).

### 3.3. Fault zones

On the southern segment of the profile (near the town of Bayankhongor) an anomalous, strongly conductive feature (20–40  $\Omega\text{m}$ ; F1 on Fig. 3d) stretches vertically through the crust from the surface. Its location at the southern edge of the Hangai Dome is congruent with the South Hangai fault zone (e.g., Walker et al., 2007, 2008; Cunningham, 2001). This is a terrane boundary marked by the location of the Bayankhongor ophiolite belt (Badarch et al., 2002), the longest continuous ophiolite belt in Central Asia (Buchan et al., 2001). It marks a collisional suture zone (Buchan et al., 2001), and is possibly an extension of the Mongol–Okhotsk suture that resulted from the closure of the Mongol–Okhotsk Ocean (e.g., Van der Voo et al., 2015). Because faults and suture zones are regions of fractured, weakened crust they often have circulating fluids that act to increase their electrical conductivity (Unsworth and Rondenay, 2012). Furthermore, this is an area of significant mineralization, which contains important sources of gold and copper (Buchan et al., 2001), and a portion of the electrical signature is likely attributed to this mineralization.

An important result observed from the resistivity model is that the lower crustal conductive zone (C2) is terminated abruptly at this fault zone. This illustrates that any lower crustal fluids are confined below the Hangai Dome and the northern Hangai region, and demonstrates the importance of this fault zone as a major crustal boundary. The large faults that bound the Hangai region are attributed to terrane sutures and suspected to be lithospheric-scale (Badarch et al., 2002; Calais et al., 2003). Hence the contrasting crustal properties observed across this fault zone likely reflect the rheological differences between the strong upper crust of the cratonal Hangai block and the weaker accretionary collage composed of terranes to the south (Badarch et al., 2002; Cunningham, 2001). Furthermore, south of the fault zone moderate resistivity values (150–1000  $\Omega\text{m}$ ) extend to depths of ~150 km, indicating a much thicker lithosphere (L1).

At the southern end of the profile another anomalous conductive feature (30–100  $\Omega\text{m}$ ; F2 on Fig. 3d) is observed. This is coincident with the location of the large Bogd fault zone at the base of the Gobi Altai mountain range, which ruptured nearby in 1957 with a moment magnitude larger than 8 (e.g., Calais et al., 2003, and references therein), and represents a significant terrane boundary (Badarch et al., 2002). In contrast, the electrical signature at the northern boundary of the Hangai region (50–1000  $\Omega\text{m}$ ; F3 on Fig. 3d), as the profile passes through the diffuse eastern segments of the Bulnay fault zone, is weaker. Perhaps a strong electrical signature is absent because deformation is dispersed across a wide area. Additionally, the fault zone may be dry and locked, as expected for fault zones with large and infrequent ruptures (Unsworth and Rondenay, 2012).

### 3.4. Upper mantle structure

Directly below the Hangai Dome the upper mantle contains a large electrically conductive feature (C3) imaged at a depth of more than 70 km, with its center at 90–100 km depth and its bottom unconstrained. Increased upper mantle conductivity from hydrous olivine (Gardés et al., 2014) is inadequate to explain the observed MT data. Calculations show that in the upper mantle (at 1200 °C) a water content of >350 ppm in olivine is required to explain the low resistivities (i.e., 30  $\Omega\text{m}$ ), which is unlikely and exceeds the solubility limits (Gardés et al., 2014). Therefore other

mechanisms must be invoked. Thus this feature is interpreted as representing a shallow asthenosphere that contains partial melt and is likely a zone of melt generation. This interpretation is supported by geochemical analysis that indicates the basaltic lavas found across the Hangai Dome have originated by partial melting over prolonged periods from a single, isolated, sub-lithospheric mantle source at depths of 70–120 km (e.g., Barry et al., 2003; Hunt et al., 2012).

A bulging asthenosphere that shallows directly below the Hangai Dome, as exhibited in the resistivity model, is consistent with previous geophysical studies. Seismic tomography data detected a thin lithosphere below the central Hangai region (60–80 km) that thickened at the edges and increased to a thickness of ~200 km below the Siberian craton to the north (Tiberi et al., 2008; Petit et al., 2008). Bouguer gravity models revealed a localized low-density structure at a depth of 80–125 km below the central Hangai (Tiberi et al., 2008), coincident with the location of the conductive feature C3. Modern adjoint tomography analysis detected a continuous, broad, low-velocity zone at mantle depths above 150 km, with the lowest shear-wave velocities occurring at depths of 60–90 km (Chen et al., 2015). Furthermore, this low-velocity zone exhibited strong positive radial anisotropy (5–10%), indicating horizontal migration of melt within the uppermost mantle (Chen et al., 2015). These broad surveys image deep structures but lack fine resolution and are prone to smearing features horizontally. Despite this, these other geophysical anomalies are broadly compatible with the resistivity model and the feature C3, although its exact geometry is not well constrained by the data. Additionally, the interpretation of the feature C3 is supported because low seismic velocities, low bulk density, and low electrical resistivity can all be explained by the presence of partial melts (Unsworth and Rondenay, 2012).

If this large upper mantle conductive zone is a region of melt generation it likely has a significant melt fraction and porosity, causing it to be very unstable (e.g., Cashman and Sparks, 2013), which can perhaps account for the widespread volcanism observed in the Hangai region. Moreover, it may cause the thermal perturbation of the surrounding area, in agreement with predicted low upper mantle viscosities (Vergnolle et al., 2003).

### 3.5. Determining melt fraction

Assuming that the low-resistivity anomalies detected below the Hangai Dome are due to partial melting alone, the minimum melt fraction required to explain the MT data can be determined. Following the two-step approach of Comeau et al. (2016), pure melt resistivity is estimated and combined with rock matrix resistivity using a two-phase equation, giving the melt fraction (by volume) necessary to explain the observed bulk resistivity (from melt + rock matrix).

Pure melt resistivity is controlled by temperature, pressure, and melt composition, primarily the silica, sodium, and water content (Nover, 2005). With accurate geochemical and thermobarometry estimates melt resistivity can be calculated by using equations derived from experimental data (e.g., Pommier and Le Trong, 2011; Laumonier et al., 2017). Geochemical analysis of lava samples from the Hangai Dome give an average composition with a silica content of  $50 \pm 4$  weight percent (wt%) and a sodium content of  $4 \pm 1$  wt% (Barry et al., 2003; Hunt et al., 2012). Determining water content can be difficult, but values of 1–6 wt% are feasible (Laumonier et al., 2017), and do not exceed solubility limits (Newman and Lowenstern, 2002). Furthermore, using low resistivity values in the analysis allows the calculation of a minimum melt fraction. Thermobarometry estimates from garnet and xenolith samples give temperatures of 1070–1200 °C for upper-most mantle depths of 60–80 km (Barruol et al., 2008; Barry et al., 2003;

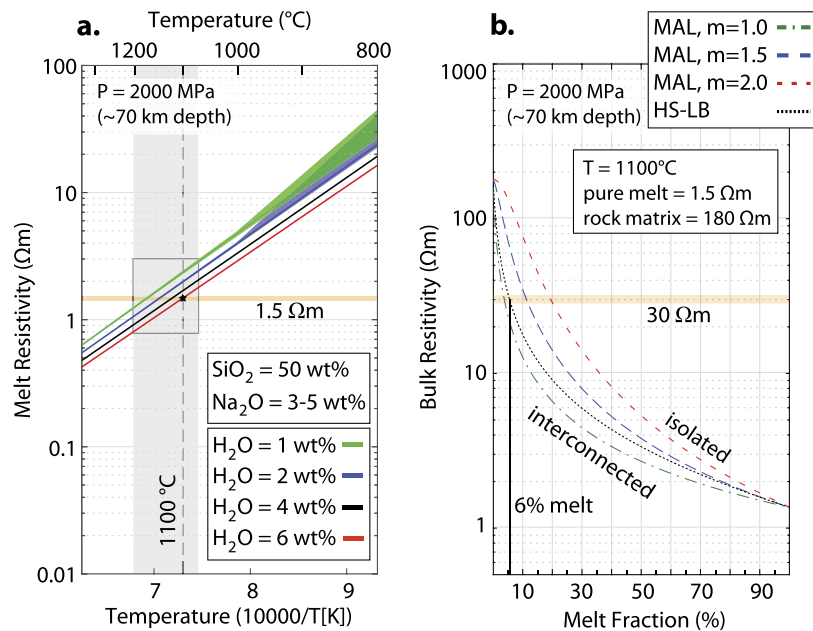


**Fig. 5.** (a) Variation of pure melt resistivity for a range of possible parameters, at  $\sim 70$  km depth (pressure of  $\sim 2000$  MPa). This includes: temperatures ( $1070$ – $1200^\circ\text{C}$ , gray bar), water contents ( $\text{H}_2\text{O}$ ;  $1$ – $6$  wt%, colors), and sodium contents ( $\text{Na}_2\text{O}$ ; range of  $3$ – $5$  wt%). Note for sodium contents the top of the range =  $5$  wt%, solid line =  $4$  wt%, and the bottom of the range =  $3$  wt% (the range is not visible for high water contents). Silica content ( $\text{SiO}_2$ ) is fixed at  $50$  wt%. The resistivity data were computed using the SIGMELTS algorithm of Pommier and Le Trong (2011). The range of all possible values are indicated by the gray box and the typical temperature is marked with a dashed gray line. The typical value, indicated by the star, gives a pure melt resistivity of  $\sim 1.5 \Omega\text{m}$  (horizontal orange line). (b) Bulk resistivity of a partially molten rock as a function of melt fraction. Dashed colored lines show the bulk resistivity computed using the modified Archie's law (MAL) (Glover et al., 2000) for various degrees of melt interconnection, from highly interconnected ( $m = 1.0$ ) to isolated ( $m = 2.0$ ). The dotted black line shows the Hashin-Shtrikman lower-resistivity bound (HS-LB) (Hashin and Shtrikman, 1962), which is representative for interconnected upper-most mantle melts. A bulk resistivity of  $30 \Omega\text{m}$  requires a minimum melt fraction of  $6\%$  (black line). (For interpretation of the references to color in this figure, the reader is referred to the web version of this article.)

Harris et al., 2010) and  $800$ – $880^\circ\text{C}$  for lower crustal depths of  $30$ – $50$  km (Barrois et al., 2008; Ionov, 2002). For a typical composition and temperature the melt resistivity algorithm SIGMELTS (Pommier and Le Trong, 2011) estimated a pure melt resistivity of  $\sim 1.5 \Omega\text{m}$  for a depth of  $\sim 70$  km (Fig. 5a). Other melt resistivity equations (e.g., Laumonier et al., 2017) gave similar results.

To calculate the melt fraction required to explain the bulk resistivity observed, a two-phase equation is used to combine the resistivity estimate of the pure melt and the rock matrix. This study uses both the modified Archie's law (Glover et al., 2000) and the Hashin-Shtrikman equation (Hashin and Shtrikman, 1962), because they both allow electrical conduction through the rock matrix, which becomes significant at high temperatures. The resistivity of the rock matrix itself was computed using the experimental resistivity-temperature relation of Hashim et al. (2013). This relation gave a resistivity of  $180 \Omega\text{m}$  for the rock matrix at  $\sim 70$  km depth, assuming a temperature of  $1100^\circ\text{C}$ . The melt geometry can be modeled as highly interconnected, by using a cementation factor of  $m = 1.0$  in Archie's law, or the melt can be located in isolated pores, using  $m = 2.0$  in Archie's law (Glover et al., 2000). The Hashin-Shtrikman lower-resistivity bound is preferred because it is thought to represent normal interconnection for upper-most mantle melts (Unsworth and Rondenay, 2012).

Assuming a bulk resistivity of  $30 \Omega\text{m}$ , typical of the conductive anomalies observed, a minimum melt fraction of  $6\%$  is required to explain the electrical resistivity data of the upper mantle conductive feature C3 (Fig. 5b). This is certainly a significant amount of melt, potentially reaching the melt connectivity transition (Rosenberg and Handy, 2005), and enough to initiate intraplate volcanism (e.g., Cashman and Sparks, 2013, and references therein). The melt fraction determined here from electrical resistivity data is in agreement with prior petrological studies that estimated  $2$ – $7\%$  melting at depths of  $70$ – $120$  km (Hunt et al., 2012) and possibly up to  $12\%$  (Barry et al., 2003).

Depending on the temperature assumed ( $1200$ – $1070^\circ\text{C}$ ), a range of melt fractions are possible ( $3.5$ – $7.5\%$ ). If higher values of pure melt resistivity are used, for example caused by a lower water content or a lower sodium content, then a higher melt fraction is required. A water content of  $1$  wt% requires  $9\%$  melt (range of  $5$ – $11\%$ ). For a moderately interconnected melt geometry the required melt fraction increases significantly to  $12\%$  (range  $8$ – $15\%$ ). A similar analysis (Fig. S7) determined that the lower crustal conductive zone (i.e., C2) could be explained by comparable melt fractions. Although for the lower crust, aqueous fluids can also explain the observed low-resistivity values, and are much more likely, as discussed above.

### 3.6. Constraints on uplift mechanisms

The MT-derived resistivity model (Fig. 3d) gives new constraints on the structure beneath the Hangai Dome. With the addition of other geophysical and geochemical evidence it is possible to critically examine mechanisms for the intra-continental uplift and support of the Hangai Dome and its associated intraplate volcanism.

A high heat-flux, deep-rooted mantle plume could explain the origin of the Hangai Dome because it would cause lithospheric thinning, uplift, and intraplate volcanism (e.g., Windley and Allen, 1993; Chen et al., 2015). It is possible that a mantle plume was active in the past, for example during early volcanism as proposed by Barry et al. (2003), but has waned, because petrological evidence indicates dispersed, low-volume volcanism lacking age progression, which is inconsistent with this mechanism (Barry et al., 2003). Furthermore, fast seismic velocities observed at depths greater than  $200$  km (Chen et al., 2015) indicate a cold mantle, perhaps from ancient subducted materials, rather than a deep mantle plume. In this study, the geometry of the upper mantle structures, as imaged in the resistivity model, do not exclude a plume-type source. However the moderate resistivity values observed disagree with very

large amounts of partial melting, contradicting a mantle plume with a very large temperature anomaly.

A thick layer (<20 km) of underplated basalt could explain crustal thickening as well as uplift and volcanism (Petit et al., 2002; Chen et al., 2015; McKenzie, 1984). However, this hypothesis is excluded by the resistivity model presented here because the expected electrical signature of a sub-crustal, homogeneous, very low-resistivity zone (Wannamaker et al., 2008) is not observed. Furthermore, the temperature estimated at the base of the crust (<900 °C) is not anomalously elevated and is inconsistent with underplated basalt (Ionov, 2002).

Uplift and doming in western Mongolia due to dynamic topography, where topography is due to an upwelling produced by flow within the mantle (as in Flament et al., 2012), is consistent with the mantle flow models of Becker and Facenna (2011). Dynamic topography as an explanation for the uplift of the Hangai Dome is not explicitly ruled out by the resistivity model. However, any mantle upwelling depicted in the resistivity model has a much smaller wavelength (<250 km) than that predicted by most dynamic topography models (>1000 km).

It is possible that a small-scale (~100 km wide) upwelling could be caused by hot and buoyant asthenospheric material replacing lithospheric material due to convective removal of the lithosphere or lithospheric removal as the result of an instability (Barry et al., 2003; Hunt et al., 2012). Alternatively, edge-driven convection influenced by a substantial lithospheric step (>100 km), between central Mongolia and the Siberian craton, could have triggered lithospheric erosion and removal (e.g., Bao et al., 2014). The low resistivity values of the upper mantle in the model presented here give compelling evidence for such a small-scale asthenospheric upwelling, and, through melt generation, it could explain the volcanism of the Hangai region and explain intra-continental uplift and doming via thermal support.

### 3.7. Melt and fluid genesis

We propose the origin of intraplate volcanism observed on the Hangai Dome arises from partial melts (>3%) generated due to decompression melting from an asthenospheric upwelling below the Hangai Dome, at a location near C3 (70–100 km depth). Melt migrating laterally within the upper mantle and excess heat cause thermal modification over a large area below the Hangai region, supporting intra-continental uplift (Chen et al., 2015; Barry et al., 2003). Other geophysical data support this model (e.g., Chen et al., 2015; Tiberi et al., 2008) and geochemical constraints from mantle xenoliths erupted in past volcanic events are in agreement (e.g., Ionov, 2002). However what initiated the process remains speculative.

We suggest that the thermally perturbed lower crust undergoes metamorphic dehydration and devolatilization reactions that create fluids which pool in isolated batches and are trapped below the brittle ductile transition. One potential explanation for the intermittent intraplate volcanism observed across the Hangai Dome is that as fluids and volatiles increase in the lower crust, local percolation thresholds are reached, triggering the ascent of underlying mantle melt (e.g., Cashman and Sparks, 2013, and references therein). Ascent is facilitated by pre-weakened upper crustal regions, allowing fast penetration and easy passage for magma directly to the surface. Mantle melt can be discharged periodically in this way.

## 4. Conclusions

The 2-D electrical resistivity model presented here, derived from MT data, offers new insights into the structure and development of the Hangai Dome. Critically, it provides new compelling

evidence that the crust beneath the Hangai region is not a homogeneous, strong, block, but rather contains a weak lower layer. Whereas the upper crust is generally highly resistive, as expected for a cratonic block, the lower crust (30–50 km) consists of a dominant low-resistivity zone, which indicates the presence of fluids. This has significant implications for crustal mechanical strength, which is required for accurate modeling of lithosphere dynamics. However, south of the Hangai Dome a clear transition in crustal properties is revealed at the prominent South Hangai fault zone and ophiolite belt, highlighting the importance of this area as a major crustal boundary. Beneath the Hangai Dome in the shallow crust, past magma ascent and eruption events have left their electrical signatures due to hydrothermal alteration. Their positions can be matched to surface expressions of volcanism and hydrothermal activity. The resistivity model images a bulging asthenosphere that shallows directly below the Hangai Dome (~70 km depth). This low-resistivity feature requires the presence of at least 3% melt, and has been identified as the magma source for observed volcanism. Thus, the Hangai intraplate volcanism can be attributed to decompression melting within a small-scale asthenospheric upwelling, which acts to support uplift of the Hangai Dome.

## Acknowledgements

This research was financially supported by the DFG (grant # BE 5149/6-1) and the SNF (grant # 200021L\_162660/1). We thank the reviewers for their comments and suggestions. We thank Thomas Kalscheuer for providing the 2-D MT inversion code. We thank Gary McNeice and Alan Jones for their tensor decomposition program. We thank the Geophysical Instrument Pool Potsdam (GIPP) for the use of their MT instruments. Additional explanatory details can be obtained in the accompanied Supplementary Material document. The MT data collected are archived and can be accessed by contacting the German Research Centre for Geosciences. We thank those who helped collect the data and provided field support, including: Sandra Grazioli, Dominic Harpering, Robin Mann, Joerg Schmalzl, Dorian Soergel, Neeraj Sudhir. A special thanks to our Mongolian colleagues for their support, including: Batbileg, Bayanjargal, Eldev-Ochir, Gantsogt, Nasan-Ochir, Nomuu, Tsagaansukh, Tserendug, Zagdsuren, and others from the Mongolian Academy of Sciences.

## Appendix A. Supplementary material

Supplementary material related to this article can be found online at <https://doi.org/10.1016/j.epsl.2018.02.007>.

## References

- Aivazpourporgou, S., Thiel, S., Hayman, P.C., Moresi, L.N., Heinson, G., 2015. Decompression melting driving intraplate volcanism in Australia: evidence from magnetotelluric sounding. *Geophys. Res. Lett.* 42, 346–354.
- Badarch, G., Cunningham, W.D., Windley, B.F., 2002. A new subdivision for Mongolia: implications for the Phanerozoic crustal growth of Central Asia. *J. Asian Earth Sci.* 21, 87–110.
- Bao, X., Eaton, D., Guest, B., 2014. Plateau uplift in western Canada caused by lithospheric delamination along a craton edge. *Nat. Geosci.* 7, 830–833.
- Barry, T.L., Saunders, A.D., Kempton, P.D., Windley, B.F., et al., 2003. Petrogenesis of cenozoic basalts from Mongolia: evidence for the role of asthenospheric versus metasomatized lithospheric mantle sources. *J. Petrol.* 44, 55–91.
- Barrool, G., Deschamps, A., Deverchere, J., Mordinova, V., et al., 2008. Upper mantle flow beneath and around the Hangay dome, Central Mongolia. *Earth Planet. Sci. Lett.* 274, 221–233.
- Becker, T.W., Facenna, C., 2011. Mantle conveyor beneath the Tethyan collisional belt. *Earth Planet. Sci. Lett.* 310, 453–461.
- Buchan, C., Cunningham, D., Windley, B.F., Tomurhuu, D., 2001. Structural and lithological characteristics of the Bayankhongor Ophiolite Zone, Central Mongolia. *J. Geol. Soc.* 158, 445–460.

- Calais, E., Vernolle, M., San'kov, V., Lukhnev, A., et al., 2003. GPS measurements of crustal deformation in the Baikal–Mongolia area (1994–2002): implications for current kinematics of Asia. *J. Geophys. Res.* 108, 1–14.
- Cashman, K.V., Sparks, R.S.J., 2013. How volcanoes work: a 25 year perspective. *Geol. Soc. Am. Bull.* 125 (5–6), 664–690.
- Chave, A.D., Jones, A.G. (Eds.), 2012. The Magnetotelluric Method: Theory and Practice. Cambridge University Press, Cambridge. 552 p.
- Chen, M., Niu, F., Liu, Q., Tromp, J., 2015. Mantle-driven uplift of Hangai Dome: new seismic constraints from adjoint tomography. *Geophys. Res. Lett.* 42.
- Comeau, M.J., Unsworth, M.J., Cordell, D., 2016. New constraints on the magma distribution and composition beneath Volcán Uturuncu and the southern Bolivian Altiplano from magnetotelluric data. *Geosphere* 12 (5), 1391–1421.
- Connolly, J.A.D., Podlachikov, Y.Y., 2004. Fluid flow in compressive tectonic settings: implications for midcrustal seismic reflectors and downward fluid migration. *J. Geophys. Res.* 109 (B4).
- Cunningham, W.D., 2001. Cenozoic normal faulting and regional doming in the southern Hangay region, Central Mongolia: implications for the origin of the Baikal rift province. *Tectonophysics* 331, 389–411.
- Deverchere, J., Petit, C., Gileva, N., Radziminovitch, N., Melnikova, V., Sankov, V., 2001. Depth distribution of earthquakes in the Baikal rift system and its implications for the rheology of the lithosphere. *Geophys. J. Int.* 146, 714–730.
- Flament, N., Gurnis, M., Muller, R.D., 2012. A review of observations and models of dynamic topography. *Lithosphere* 5 (2), 189–210.
- Ganbat, E., Demberel, O., 2010. Geologic background of the Hangay geothermal system, West-Central Mongolia. In: Proceedings of the World Geothermal Congress 2010. Bali, Indonesia, 25–29 April 2010.
- Gardés, E., Gaillard, F., Tarits, P., 2014. Toward a unified hydrous olivine electrical conductivity law. *Geochem. Geophys. Geosyst.* 15, 4984–5000.
- Glover, P., Hole, M.J., Pous, J., 2000. A modified Archie's Law for two conducting phases. *Earth Planet. Sci. Lett.* 180, 369–383.
- Grayver, A.V., Kuvshinov, A.V., 2016. Exploring equivalence domain in nonlinear inverse problems using Covariance Matrix Adaption Evolution Strategy (CMAES) and random sampling. *Int. J. Geophys.* 205, 971–987.
- Harris, N., Hunt, A., Parkinson, I., Tindle, A., Yondon, M., Hammond, S., 2010. Tectonic implications of garnet-bearing mantle xenoliths exhumed by Quaternary magmatism in the Hangay dome, central Mongolia. *Contrib. Mineral. Petrol.* 160, 67–81.
- Hashim, L., Gaillard, F., Champallier, R., Le Breton, N., Arbaret, L., Scaille, B., 2013. Experimental assessment of the relationships between electrical resistivity, crustal melting and strain localization beneath the Himalayan–Tibetan Belt. *Earth Planet. Sci. Lett.* 373, 20–30.
- Hashin, Z., Shtrikman, S., 1962. A variational approach to the elastic behavior of multiphase minerals. *J. Mech. Phys. Solids* 11, 127–140.
- Hill, G.J., Caldwell, T.G., Heise, W., Chertkoff, D.G., et al., 2009. Distribution of melt beneath Mount St Helens and Mount Adams inferred from magnetotelluric data. *Nat. Geosci.* 2, 785–789.
- Hunt, A.C., Parkinson, I.J., Harris, N., Barry, T.L., Rogers, N.W., Yondon, M., 2012. Cenozoic volcanism on the Hangai Dome, Central Mongolia: geochemical evidence for changing melt sources and implications for mechanisms of melting. *J. Petrol.* 53 (9), 1913–1942.
- Ionov, D., 2002. Mantle structure and rifting processes in the Baikal–Mongolia region: geophysical data and evidence from xenoliths in volcanic rocks. *Tectonophysics* 351, 41–60.
- Kalscheuer, T., Juanatey, M.D.Á.G., Meqbel, N., Pedersen, L.B., 2010. Non-linear model error and resolution properties from two-dimensional single and joint inversions of direct current resistivity and radiomagnetotelluric data. *Geophys. J. Int.* 182 (3), 1174–1188.
- Laumonier, M., Gaillard, F., Muir, D., Blundy, J., Unsworth, M., 2017. Giant magmatic water reservoirs at mid-crustal depth inferred from electrical conductivity and the growth of the continental crust. *Earth Planet. Sci. Lett.* 457, 173–180.
- Liu, L., Hasterok, D., 2016. High-resolution lithosphere viscosity and dynamics revealed by magnetotelluric imaging. *Science* 353, 1515–1518.
- McKenzie, D., 1984. A possible mechanism for epeirogenic uplift. *Nature* 307, 16.
- McNeice, G.W., Jones, A.G., 2001. Multisite, multifrequency tensor decomposition of magnetotelluric data. *Geophysics* 66, 158–173.
- Munoz, G., Ritter, O., 2013. Pseudo-remote reference processing of magnetotelluric data: a fast and efficient data acquisition scheme for local arrays. *Geophys. Prospect.* 61, 300–316.
- Newman, S., Lowenstein, J.B., 2002. VolatileCalc: a silicate melt–H<sub>2</sub>O–CO<sub>2</sub> solution model written in Visual Basic for Excel. *Comput. Geosci.* 28, 597–604.
- Nover, G., 2005. Electrical properties of crustal and mantle rocks—a review of laboratory measurements and their explanation. *Surv. Geophys.* 26, 593–651.
- Oyunsetseg, D., Ganchimeg, D., Minjigmaa, A., Ueda, A., Kusakabe, M., 2015. Isotopic and chemical studies of hot and cold springs in western part of Khangai Mountain region, Mongolia, for geothermal exploration. *Geothermics* 53, 488–497.
- Petit, C., Tiberi, C., Deschamps, A., Deverchere, J., 2008. Teleseismic traveltimes, topography and the lithospheric structure across central Mongolia. *Geophys. Res. Lett.* 35, 1–5.
- Petit, C., Déverchère, J., Calais, E., Sankov, V., Fairhead, D., 2002. Deep structure and mechanical behavior of the lithosphere in the Hangai–Hövsgöl region, Mongolia: new constraints from gravity modeling. *Earth Planet. Sci. Lett.* 197, 133–149.
- Pommier, A., Le Trong, E., 2011. SIGMELTS: a web portal for electrical conductivity calculations in geosciences. *Comput. Geosci.* 37, 1450–1459.
- Ritter, O., Weckmann, U., Vietor, T., Haak, V., 2003. A magnetotelluric study of the Damara Belt in Namibia. 1. Regional scale conductivity anomalies. *Phys. Earth Planet. Inter.* 138, 71–90.
- Rosenberg, C.L., Handy, M.R., 2005. Experimental deformation of partially melted granite revisited: implications for the continental crust. *J. Metamorph. Geol.* 23, 19–28.
- Rung-Arunwan, T., Siripunvaraporn, W., Utada, H., 2016. On the Berdichevsky average. *Phys. Earth Planet. Inter.* 253, 1–4.
- Sahagian, D., Prousevitch, A., Ancuta, L.D., Idleman, B.D., Zeitler, P.K., 2016. Uplift of central Mongolia recorded in vesicular basalts. *J. Geol.* 124 (4), 435–445. <https://doi.org/10.1086/686272>.
- Tiberi, C., Deschamps, A., Déverchère, J., Petit, C., Perrot, J., Appriou, D., 2008. Asthenospheric imprints on the lithosphere in Central Mongolia and Southern Siberia from a joint inversion of gravity and seismology (MOBAL experiment). *Geophys. J. Int.* 175, 1283–1297.
- Unsworth, M.J., Rondenay, S., 2012. Mapping the distribution of fluids in the crust and lithospheric mantle utilizing geophysical methods. In: Harlov, D.E., Aus- trheim, H. (Eds.), Metasomatism and the Chemical Transformation of Rock. In: Lecture Notes in Earth System Sciences. Springer-Verlag, Berlin, pp. 535–598.
- Van der Voo, R., van Hinsbergen, D.J.J., Domeier, M., Spakman, W., Torsvik, T.H., 2015. Latest Jurassic–earliest Cretaceous closure of the Mongol–Okhotsk Ocean: a paleomagnetic and seismological-tomographic analysis. *Spec. Pap., Geol. Soc. Am.* 513.
- Vergnolle, M., Pollitz, F., Calais, E., 2003. Constraints on the viscosity of the continental crust and mantle from GPS measurements and postseismic deformation models in western Mongolia. *J. Geophys. Res.* 108.
- Walker, R.T., Nissen, E., Molor, E., Bayasgalan, A., 2007. Reinterpretation of the active faulting in central Mongolia. *Geology* 35, 759–762.
- Walker, R.T., Molor, E., Fox, M., Bayasgalan, A., 2008. Active tectonics of an apparently aseismic region: distributed active strike-slip faulting in the Hangay Mountains of central Mongolia. *Geophys. J. Int.* 174, 1121–1137.
- Wannamaker, P.E., Hasterok, D.P., Johnston, J.M., Stodt, J.A., et al., 2008. Lithospheric dismemberment and magmatic processes of the Great Basin–Colorado Plateau transition, Utah, implied from magnetotellurics. *Geochem. Geophys. Geosyst.* 9.
- Windley, B.F., Allen, M.B., 1993. Mongolian plateau: evidence for a late Cenozoic mantle plume under central Asia. *Geology* 21, 295–298.